A MASTER′S THESIS

A NUMERICAL ANALYSIS OF TWO LAYER CURRENT OF FISHERY PORT WITH MANIFOLD CHANNEL

JEJU NATIONAL UNIVERSITY GRADUATE SCHOOL

Department of Civil & Ocean Engineering

Chang-Lym Lee

February 2010

A NUMERICAL ANALYSIS OF TWO LAYER CURRENT OF FISHERY PORT WITH MANIFOLD CHANNEL

Chang-Lym Lee

(Supervised by Professor Nam-Hyeong Kim)

A thesis submitted in partial fulfillment of the requirement for the Degree of Master of Engineering

2010. 2

Department of Civil & Ocean Engineering

GRADUATE SCHOOL

JEJU NATIONAL UNIVERSITY

CONTENTS

List of Figures

List of Tables

Summary

Due to the rapid worldwide growth of international trade and commerce and to the fact that modern ships are larger, ports and harbors must therefore increase the depth of their fairways in order to maintain or enhance their economic competitiveness. This would definitely facilitate commercial and economic growth but the port activities are also likely to cause deterioration of air and marine water quality in the surrounding areas. A port can lead to severe pollution problem, over a large area due to the multifarious activities.

Recently, as a concern of Eco-port is increased internationally, the improvement of water quality at the harbor or fishery port has gained increasing importance. Therefore, several methods have been studied to improve the water quality at the harbor or fishery port, and SEB (Seawater Exchange Breakwater) has been focused among these study. SEB is the structure established at the breakwater for exchanging the water of inside area with the seawater from outside. It, then, has greatly improved the water quality on the port where the SEB has been established (Han and Lee, 2006). But it has been shown a problem that the water on the inside area that is far from the SEB cannot be exchanged well, so that the water quality on that area has been still poor.

In this study, to solve the problem of the SEB, Manifold channel, a new concept of SEB, is applied at the fishery port to exchange the water on the inside area. By using the manifold channels, it is possible to exchange the water on the inside area, where cannot be exchanged by the SEB, with the seawater from outside. In addition, it can be prevented partial eddies, which might be occurred by the SEB, by controlling gate conditions of manifold channels.

To compare Manifold channel with previous SEB, a numerical model by two layer current of Jumunjin fishery port where the SEB has been established is carried out, and the computed results are compared with observed data to verify this model. Also, virtual manifold channels are assumed on Jumunjin fishery port, and the two layer current model is carried out under the same condition as the SEB. And then it is examined that Manifold channel has an advantage over the SEB for the water exchange on the inside area.

The results of these comparisons are shown that Manifold channel has an advantage over the SEB for the water exchange on the inside area. Also, to examine the effect of gate conditions in Manifold channel, five cases of manifold channels are established on Jumunjin fishery port, and the two layer current model is carried out. From these results, the suitable outflow gate positions of the manifold channels are identified.

In the future, the study on the detailed outflow gate positions will be continued, also, to improve the numerical analysis of the flow domain, this model will be developed as multi-layer current. Therefore, Manifold channel might be used broadly for the design of a breakwater to develop the facilities of port with waterfront area and water amenity.

CHAPTER 1
INTRODUCTON

1.1 Background

More than 50% of the world population lives close to the coast, of which more than 300 million inhabit the coastal urban areas. Entering the 21st century, there are significant increases in maritime trade among various countries. To meet the increasing demands of population and requirements of the industries, new ports are being constructed or existing ports are being expanded throughout the world. This would definitely facilitate commercial and economic growth but the port activities are also likely to cause deterioration of air and marine water quality in the surrounding areas. A port can lead to severe pollution problem, over a large area due to the multifarious activities.

Recently, as the concern of Eco-port is increased internationally, the improvement of water quality at the harbor or fishery port has gained increasing importance. Therefore, several methods have been studied to improve the water quality at the harbor or fishery port, and SEB (Seawater Exchange Breakwater) has been focused among these study in recent year. SEB is the structure established at the breakwater for exchanging water of inside area with seawater from outside. It, then, has greatly improved the water quality on the port where SEB has been established (Han and Lee, 2006). But it has been shown a problem that the water on the inside area that is far from the SEB cannot be exchanged well, so that the water quality on that area has been still poor.

In this study, to solve the problem of SEB, Manifold channel, a new concept of SEB, is introduced. By using the manifold channels, it is possible to exchange the water on the inside area, where cannot be exchanged by SEB, with seawater from outside. Therefore, the contaminated water of inside area can be exchanged by the seawater from outside, throughout

the port. Also, it can be prevented partial eddies, which may be occurred by the SEB, by controlling gate conditions of manifold channel.

1.2 Objectives

In recent years, as the concern of Eco-port is increased internationally, the improvement of water quality at the harbor or fishery port has gained increasing importance. Therefore, SEB is often applied for improving water quality at the harbor or fishery port. But it still has problem that the water at the inside area that is far from the SEB cannot be exchanged well. Accordingly, the main objectives of this study are to exchange the water of inside area, where cannot be exchanged by the SEB, with the seawater from outside area. Therefore, Manifold channel, a new concept of SEB, is proposed, the effect of the water exchanging on the inside area by Manifold channel is investigated. By using numerical simulation, the suitable conditions and aspect of Manifold channel can be designed.

1.3 Study contents

A numerical analysis of two layer current by finite element method is described in this study. To verify this numerical analysis and to investigate Manifold channel, the numerical model by two layer current of Jumunjin fishery port where the SEB has been established is carried out. Also, virtual manifold channels are assumed on Jumunjin fishery port, and the two layer current model is simulated to examine the effect of Manifold channel. The six chapters consist as follows:

In Chapter 1, the background and the purposes of this study are given.

In Chapter 2, the finite element methods solving the primitive variables of incompressible flows are discussed and the basic equations of two layer current are explained.

In Chapter 3, to apply two layer model, the moving boundary is applied to this model, and it is described.

In Chapter 4, the numerical model by two layer current of Jumunjin fishery port is performed by two cases; Case 1 is computed for tidal current and Case 2 is established SEB. And the numerical results are compared with the observed data to verify this model.

In Chapter 5, the numerical analysis conditions and the information of the manifold channels are described, and the numerical model of Jumunjin fishery port with virtual manifold channels is simulated. Also, to examine the effect of gate condition in Manifold channel, five cases of manifold channels are assumed and the numerical model is simulated.

In Chapter 6, the main achievements of present study are prescribed, and some remained problems are discussed.

CHAPTER 2
FORMULATIONS OF FINITE ELEMENT ANALYSIS

Many numerical methods have been proposed for incompressible flows. In this chapter, the finite element methods solving the primitive variables of incompressible flows are discussed and the basic equations of two layer current are explained as follows.

2.1 Shallow Water Equation

The non-linear shallow water equation is applied to calculate the water behavior. The shallow water equation consists of the Navier-stokes equation and the Euler's equation of continuity, which can be written as follows:

$$\dot{U} + U_j U_{i,j} + g\eta_{,i} - \nu_e\left(U_{i,j} + U_{j,i}\right)_{,j} + \alpha_b U_i = 0 \tag{1}$$

$$\frac{\partial \eta}{\partial x} + \{(b+\eta)U_i\}_{,i} = 0 \tag{2}$$

where, U is averaged velocity, η is the water elevation from the mean sea level, b is the depth from the mean sea level to the sea bed, g is the gravity acceleration, ν_e is the eddy viscosity, respectively. The friction on the bed is considered by linear and expressed as follows:

$$\alpha_b = \frac{f_b}{(b+\eta)\rho}\sqrt{U_k U_k} \tag{3}$$

where, f_b is the friction on the bed.

2.2 Boundary Conditions

The initial condition in an actual coastal zone is difficult to know, the computation starts with the calm sea domain is assumed as the initial boundary condition.

$$\left.\begin{array}{l} \eta = \hat{\eta}_0 \\ U_i = \hat{U}_{i0} \end{array}\right\} \quad at \;\; t = 0 \tag{4}$$

The boundary conditions are shown in Fig.1 and it can be defined as

$$U_n = 0 \qquad on \;\; \Gamma_L \tag{5}$$

$$\eta = \hat{\eta} \qquad on \;\; \Gamma_O \tag{6}$$

where the subscript n refers to a normal velocity to the coastline and $\hat{\eta}$ is the temporary surface elevation at each time.

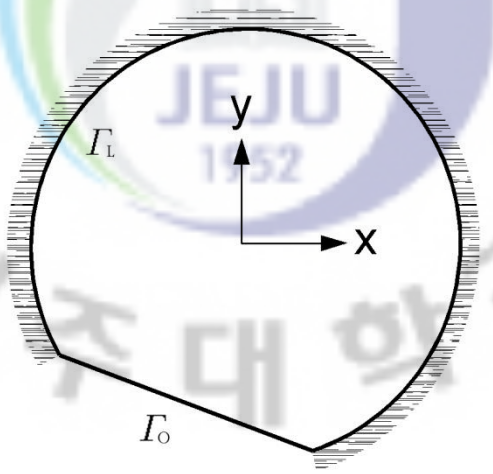

Fig. 1 Boundary conditions

2.3 Basic Equations of Two Layer Current

The coordinates X, Y, Z are illustrated in Fig. 2. In the subsequent development of the two layer current equations, the following notation will be used: U and V are the velocities of the upper and lower layer, η is the water elevation from the mean sea level, b is the depth from the mean sea level to the sea bed, and d is the depth from the mean sea level to interface level, respectively.

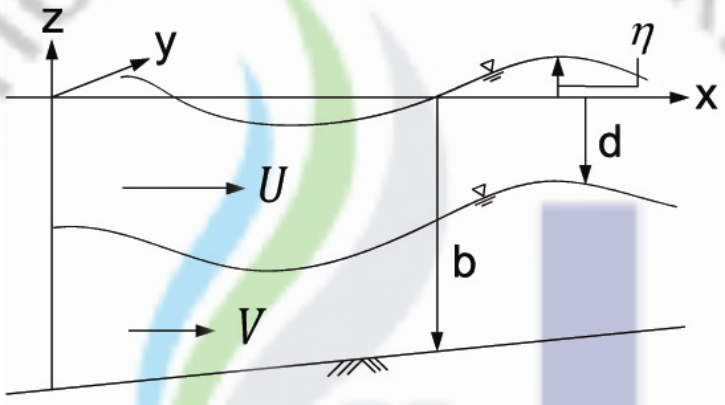

Fig. 2 Two layer model

To obtain the continuity equation of two layer model, Euler's equation of continuity is integrated over the depth of the upper layer vertically, which is expressed by

$$\int_{-d}^{\eta}\left(\frac{\partial u}{\partial x}+\frac{\partial v}{\partial y}+\frac{\partial w}{\partial z}\right)dZ=0 \tag{7}$$

Application of Leibnitz' rule for interchanging the order of differentiation and integration in the first two integrals and direct evaluation of the third integral yield the following equation:

$$\left.\begin{aligned}\frac{\partial}{\partial x}\int_{-d}^{\eta}udZ+\frac{\partial}{\partial y}\int_{-d}^{\eta}vdZ+\left(w_\eta-u_\eta\frac{\partial\eta}{\partial x}-v_\eta\frac{\partial\eta}{\partial y}\right)\\-\left(w_d+u_d\frac{\partial d}{\partial x}+v_d\frac{\partial d}{\partial y}\right)=0\end{aligned}\right\} \tag{8}$$

When the three-dimensional flow equations are integrated over the depth, the need arises for conditions on the flow at the surface, interface and bottom. If the equation of boundary is $F(x, y, z, t) = 0$, then at every point on the boundary we must have the equation as follows:

$$\frac{DF}{Dt} = \frac{\partial F}{\partial t} + u\frac{\partial F}{\partial x} + v\frac{\partial F}{\partial y} + w\frac{\partial F}{\partial z} = 0 \tag{9}$$

The boundary condition at the surface is $Z = \eta(x, y: t) = 0$, which can be expressed by

$$F(x, y, z: t) = Z - \eta(x, y: t) = 0 \tag{10}$$

Substituting Eq. (10) into Eq. (9) yields the following equation:

$$\frac{\partial \eta}{\partial t} + u_\eta \frac{\partial \eta}{\partial x} + v_\eta \frac{\partial \eta}{\partial y} = w_\eta \qquad at\ Z = \eta \tag{11}$$

The boundary condition at the interface is $z = -d(x, y: t)$, which can be expressed by

$$F(x, y, z: t) = z + d(x, y, : t) = 0 \tag{12}$$

Substituting Eq. (12) into Eq. (9), leads to

$$\frac{\partial d}{\partial t} + u_d \frac{\partial d}{\partial x} + v_d \frac{\partial d}{\partial y} = -w_d \qquad at\ Z = -d \tag{13}$$

Boundary conditions Eq. (11) and Eq. (13) can be applied to Eq. (8) to reduce it to the form as following equation:

$$\frac{\partial}{\partial t}(\eta + d) + \frac{\partial}{\partial x}\int_{-d}^{\eta} u\, dZ + \frac{\partial}{\partial y}\int_{-d}^{\eta} v\, dZ = 0 \tag{14}$$

The U and V of the vertically averaged velocity of the upper layer are defined by

$$U = \frac{1}{\eta + d}\int_{-d}^{\eta} u\, dZ \tag{15}$$

$$V = \frac{1}{\eta + d}\int_{-d}^{\eta} v\, dZ \tag{16}$$

Substituting Eqs. (15) and (16) into Eq. (14), results in

$$\frac{\partial}{\partial t}(\eta + d) + \frac{\partial}{\partial x}\{U(\eta + d)\} + \frac{\partial}{\partial y}\{V(\eta + d)\} = 0 \tag{17}$$

By using Einstein notation, the continuity equation of the upper layer is rewritten as follows:

$$\dot{\eta} + \dot{d} + \{U_i(\eta + d)\}_{,i} = 0 \tag{18}$$

From an analogous development of the upper layer, for the lower layer, Euler's equation of continuity is vertically integrated over the depth of the lower layer, which is expressed by

$$\int_{-b}^{-d}\left(\frac{\partial u}{\partial x} + \frac{\partial v}{\partial y} + \frac{\partial w}{\partial z}\right) dZ = 0 \tag{19}$$

Application of Leibnitz' rule for interchanging the order of differentiation and integration in the first two integrals and direct evaluation of the third integral yield the following equation:

$$\left.\begin{aligned} &\frac{\partial}{\partial x}\int_{-b}^{-d} u\, dZ + \frac{\partial}{\partial y}\int_{-b}^{-d} v\, dZ + \left(w_d + u_d\frac{\partial d}{\partial x} + v_d\frac{\partial d}{py}\right) \\ &\qquad -\left(w_b + u_b\frac{\partial b}{\partial x} + v_b\frac{\partial b}{\partial y}\right) = 0 \end{aligned}\right\} \tag{20}$$

The boundary condition at the interface is $Z = -d(x, y: t) = 0$, which can be expressed by

$$F(x, y, z: t) = Z + d(x, y: t) = 0 \tag{21}$$

Substituting Eq. (21) into Eq. (9) yields the following equation:

$$\frac{\partial d}{\partial t} + u_d \frac{\partial d}{\partial x} + v_d \frac{\partial d}{\partial y} = -w_d \qquad at\ Z = -d \tag{22}$$

The boundary condition at the bottom is $z = -b(x, y)$, which can be expressed by

$$F(x, y, z: t) = Z + b(x, y) = 0 \tag{23}$$

Substituting Eq. (23) into Eq. (9), leads to

$$u_b \frac{\partial b}{\partial x} + v_b \frac{\partial b}{\partial y} = -w_b \qquad at\ Z = -b \tag{24}$$

Boundary conditions Eqs. (22) and (24) can be applied to Eq. (20) to reduce it to the form as following equation:

$$-\frac{\partial d}{\partial t} + \frac{\partial}{\partial x}\int_{-b}^{-d} u\, dZ + \frac{\partial}{\partial y}\int_{-b}^{-d} v\, dZ = 0 \tag{25}$$

The U and V of the vertically averaged velocity of the lower layer are defined by

$$U = \frac{1}{b-d}\int_{-b}^{-d} u\, dZ \tag{26}$$

$$V = \frac{1}{b-d}\int_{-b}^{-d} v\, dZ \tag{27}$$

Substituting Eqs. (15) and (16) into Eq. (14), results in

$$-\frac{\partial d}{\partial t} + \frac{\partial}{\partial x}\{U(b-d)\} + \frac{\partial}{\partial y}\{V(b-d)\} = 0 \tag{28}$$

By using Einstein notation, the continuity equation of lower layer is therefore

$$\dot{d} + \{V_i(d-b)\}_{,i} = 0 \tag{29}$$

The equations of motion in the x, y and z directions are described by the Navier-Stokes equations as follows:

$$\frac{\partial u}{\partial t} + u\frac{\partial u}{\partial x} + v\frac{\partial u}{\partial y} + w\frac{\partial u}{\partial z} + \frac{1}{\rho}\frac{\partial P}{\partial x} - \frac{1}{\rho}\left(\frac{\partial \tau_{xx}}{\partial x} + \frac{\partial \tau_{xy}}{\partial y} + \frac{\partial \tau_{xz}}{\partial z}\right) = 0 \tag{30}$$

$$\frac{\partial v}{\partial t} + u\frac{\partial v}{\partial x} + v\frac{\partial v}{\partial y} + w\frac{\partial v}{\partial z} + \frac{1}{\rho}\frac{\partial P}{\partial y} - \frac{1}{\rho}\left(\frac{\partial \tau_{xy}}{\partial x} + \frac{\partial \tau_{yy}}{\partial y} + \frac{\partial \tau_{yz}}{\partial z}\right) = 0 \tag{31}$$

$$\frac{\partial w}{\partial t} + u\frac{\partial w}{\partial x} + v\frac{\partial w}{\partial y} + w\frac{\partial w}{\partial z} + \frac{1}{\rho}\frac{\partial P}{\partial z} + g - \frac{1}{\rho}\left(\frac{\partial \tau_{xz}}{\partial x} + \frac{\partial \tau_{yz}}{\partial y} + \frac{\partial \tau_{zz}}{\partial z}\right) = 0 \tag{32}$$

where, u, v and w are the velocity components in the x, y and z directions, P is pressure, ρ is fluid density, τ is shear stress, g is gravity acceleration, respectively.

Navier-Stokes equations can be simplified by assuming that the vertical accelerations are negligible and that the shear stresses are negligible compared to gravity and the vertical pressure gradient. These assumptions are equivalent to stating that the pressure in the z direction is hydrostatic. Eq. (32) is then expressed as follows:

$$\frac{\partial P}{\partial Z} = -\rho g \tag{33}$$

$$P = \rho_u g(\eta - Z) \tag{34}$$

where, ρ_u is the density of the upper layer.

Substituting Eq. (34) into Eq. (30) and Eq. (31), leads to

$$\frac{\partial u}{\partial t} + u\frac{\partial u}{\partial x} + v\frac{\partial u}{\partial y} + w\frac{\partial u}{\partial z} + g\frac{\partial \eta}{\partial x} - \frac{1}{\rho_u}\left(\frac{\partial \tau_{xx}}{\partial x} + \frac{\partial \tau_{xy}}{\partial y} + \frac{\partial \tau_{xz}}{\partial z}\right) = 0 \tag{35}$$

$$\frac{\partial v}{\partial t} + u\frac{\partial v}{\partial x} + v\frac{\partial v}{\partial y} + w\frac{\partial v}{\partial z} + g\frac{\partial \eta}{\partial y} - \frac{1}{\rho_u}\left(\frac{\partial \tau_{xy}}{\partial x} + \frac{\partial \tau_{yy}}{\partial y} + \frac{\partial \tau_{yz}}{\partial z}\right) = 0 \tag{36}$$

Eq. (35) is integrated over the water depth of the upper layer and the Leibnitz' rule is applied to yield, it can be written as:

$$\left.\begin{aligned}&\int_{-d}^{\eta}\left(\frac{\partial u}{\partial t}\right)dZ+\int_{-d}^{\eta}\left(u\frac{\partial u}{\partial x}+v\frac{\partial u}{\partial y}+w\frac{\partial u}{\partial z}\right)dZ+\int_{-d}^{\eta}g\frac{\partial \eta}{\partial x}dZ\\&\qquad-\int_{-d}^{\eta}\frac{1}{\rho}\left(\frac{\partial \tau_{xx}}{\partial x}+\frac{\partial \tau_{xy}}{\partial y}\partial\tau_{xz}\partial z\right)dZ\\&=\frac{\partial}{\partial t}\int_{-d}^{\eta}udZ+\frac{\partial}{\partial x}\int_{-d}^{\eta}u^2dZ+\frac{\partial}{\partial y}\int_{-d}^{\eta}uvdZ+g\frac{\partial \eta}{\partial z}(\eta+d)\\&\qquad-\frac{1}{\rho}\int_{-d}^{\eta}\frac{\partial \tau_{xx}}{\partial x}dZ-\frac{1}{\rho}\int_{-d}^{\eta}\frac{\partial \tau_{xy}}{\partial y}dZ-\frac{1}{\rho}\int_{-d}^{\eta}\frac{\partial \tau_{xz}}{\partial z}dZ\end{aligned}\right\}\quad(37)$$

where, the first four term of Eq. (37) is given as

$$\int_{-d}^{\eta}\frac{\partial \tau_{xx}}{\partial x}dZ=\frac{\partial \tau_{xx}}{\partial x}\int_{-d}^{\eta}dZ=\frac{\partial \tau_{xx}}{\partial x}(\eta+d)\quad(38)$$

$$\int_{-d}^{\eta}\frac{\partial \tau_{xy}}{\partial y}dZ=\frac{\partial \tau_{xy}}{\partial y}(\eta+d)\quad(39)$$

$$\int_{-d}^{\eta}\frac{\partial \tau_{xz}}{\partial z}dZ=\tau_{xz\eta}-\tau_{xzd}\quad(40)$$

$$\left.\begin{aligned}&\int_{-d}^{\eta}\frac{1}{\rho_u}\left(\frac{\partial \tau_{xx}}{\partial x}+\frac{\partial \tau_{xy}}{\partial y}+\frac{\partial \tau_{xz}}{\partial z}\right)dZ\\&=\frac{1}{\rho_u}(\eta+d)\left(\frac{\partial \tau_{xx}}{\partial_x}+\frac{\partial \tau_{xy}}{\partial y}\right)+\frac{1}{\rho_u}\left(\tau_{xz\eta}-\tau_{xzd}\right)\end{aligned}\right\}\quad(41)$$

Also, the shear stresses are expressed as follows:

$$\tau_{xy}=\mu\left(\frac{\partial v}{\partial x}+\frac{\partial u}{\partial y}\right)\quad(42)$$

$$\tau_{yy}=\mu\left(\frac{\partial v}{\partial y}+\frac{\partial v}{\partial y}\right)=2\mu\frac{\partial u}{\partial y}\quad(43)$$

$$\tau_{xx}=\mu\left(\frac{\partial u}{\partial x}+\frac{\partial u}{\partial x}\right)=2\mu\frac{\partial u}{\partial x}\quad(44)$$

Also, it is assumed that the shear stresses $\tau_{xz\eta}$, $\tau_{zx\eta}$, $\tau_{yz\eta}$, $\tau_{zy\eta}$ at the surface are zero and that the shear stress at the interface is proportional to the velocity, the shear stress at the interface can be given as

$$\tau_{xzd} = \tau_{zxd} = \mu\left(\frac{\partial w}{\partial x} + \frac{\partial u}{\partial z}\right) \simeq C_b'(U_1 - V_1) \tag{45}$$

where, U_1 is the velocity component of the upper layer in the x direction and V_1 is the velocity component of the lower layer in the x direction.

Substituting Eqs. (42), (43), (44) and (45) into Eq. (41), leads to

$$\left.\begin{aligned}&\int_{-d}^{\eta}\frac{1}{\rho_u}\left(\frac{\partial \tau_{xx}}{\partial x} + \frac{\partial \tau_{xy}}{\partial y} + \frac{\partial \tau_{xz}}{\partial z}\right)dZ\\ &= \frac{1}{\rho_u}(\eta + d)\left\{\frac{\partial}{\partial x}\left(2\mu\frac{\partial u}{\partial x}\right) + \frac{\partial}{\partial y}\mu\left(\frac{\partial v}{\partial x} + \frac{\partial u}{\partial y}\right)\right\} - \frac{1}{\rho_u}C_b'(U_1 - V_1) = 0\end{aligned}\right\} \tag{46}$$

Eq. (37) is therefore expressed as

$$\left.\begin{aligned}&\frac{\partial}{\partial t}\int_{-d}^{\eta} u dZ + \frac{\partial}{\partial x}\int_{-d}^{\eta} u^2 dZ + \frac{\partial}{\partial y}\int_{-d}^{\eta} uv dZ + g\frac{\partial \eta}{\partial z}(\eta + d)\\ &-\frac{1}{\rho_u}(\eta + d)\left\{\frac{\partial}{\partial x}\left(2\mu\frac{\partial u}{\partial x}\right) + \frac{\partial}{\partial y}\mu\left(\frac{\partial v}{\partial x} + \frac{\partial u}{\partial y}\right)\right\} + \frac{1}{\rho_u}C_b'(U_1 - V_1) = 0\end{aligned}\right\} \tag{47}$$

The momentum correction coefficients of the upper layer are given as follows:

$$\beta_{xx} = \frac{1}{(\eta + d)U^2}\int_{-d}^{\eta} u^2 dZ \tag{48}$$

$$\beta_{xy} = \frac{1}{(\eta + d)UV}\int_{-d}^{\eta} uv dZ \tag{49}$$

Substituting Eq. (15), (16), (48) and (49) into Eq. (47), assuming that μ is constant for the depth in the x, y directions and that β_{xx} and β_{xy} are 1, respectively, the result is defined as follows:

$$\left.\begin{aligned} &\frac{\partial U}{\partial t}+U\frac{\partial U}{\partial x}+V\frac{\partial U}{\partial y}+g\frac{\partial \eta}{\partial x} \\ &-\nu_e^u\frac{\partial}{\partial x}\left(2\frac{\partial U}{\partial x}\right)-\nu_e^u\frac{\partial}{\partial y}\left(\frac{\partial V}{\partial x}+\frac{\partial U}{\partial y}\right)+\frac{C_b}{\eta+d}(U_1-V_1)=0 \end{aligned}\right\} \quad (50)$$

where, $C_b=\frac{C_b^{'}}{\rho_u}$ and $\nu_e^u\left(=\frac{\mu}{\rho_u}\right)$ is the eddy viscosity of the upper layer.

The stress of the interface is considered to be linear, that is expressed as follows:

$$\alpha_m=\frac{C_b}{\eta+d}=\frac{f_m}{(\eta+d)\rho_u}\sqrt{(U_1-V_1)^2+(U_2-V_2)^2} \quad (51)$$

where, f_m is the friction coefficient of the interface, U_2 is the velocity component of the upper layer in y direction and V_2 is the velocity component of the lower layer in y direction.

From an analogous development, the y component of the momentum equation can be yielded, and by using Einstein notation, the momentum equation of the upper layer is therefore obtained as follows:

$$\dot{U}+U_jU_{i,j}+g\eta_{,i}-\nu_e^u\left(U_{i,j}+U_{j,i}\right)_{,j}+\alpha_m(U_i-V_i)=0 \quad (52)$$

From Eq. (34), Eq. (32) for the lower layer is then expressed as follows:

$$P=\rho_u g(\eta+d)-\rho_l g(\eta+d) \quad (53)$$

where, ρ_l is the density of the lower layer.

By substituting Eq. (53) into Eqs. (30) and (31), the results lead to

$$\left.\begin{aligned} &\frac{\partial u}{\partial t}+u\frac{\partial u}{\partial x}+v\frac{\partial u}{\partial y}+w\frac{\partial u}{\partial z}+g\varepsilon\frac{\partial \eta}{\partial x} \\ &+g(\varepsilon-1)\frac{\partial d}{\partial x}-\frac{1}{\rho_l}\left(\frac{\partial \tau_{xx}}{\partial x}+\frac{\partial \tau_{xy}}{\partial y}+\frac{\partial \tau_{xz}}{\partial z}\right)=0 \end{aligned}\right\} \quad (54)$$

$$\left.\begin{aligned}&\frac{\partial v}{\partial t}+u\frac{\partial v}{\partial x}+v\frac{\partial v}{\partial y}+w\frac{\partial v}{\partial z}+g\varepsilon\frac{\partial \eta}{\partial y}\\&+g(\varepsilon-1)\frac{\partial d}{\partial y}-\frac{1}{\rho_l}\left(\frac{\partial \tau_{xy}}{\partial x}+\frac{\partial \tau_{yy}}{\partial y}+\frac{\partial \tau_{yz}}{\partial z}\right)=0\end{aligned}\right\} \quad (55)$$

where, $\varepsilon\left(=\frac{\rho_u}{\rho_l}\right)$ is the rate of density.

Eq. (55) is integrated over the water depth of the lower layer and the Leibnitz' rule is applied to yield, it can be written as:

$$\left.\begin{aligned}&\int_{-b}^{-d}\left(\frac{\partial u}{\partial t}\right)dZ+\int_{-b}^{-d}\left(u\frac{\partial u}{\partial x}+v\frac{\partial u}{\partial y}+w\frac{\partial u}{\partial z}\right)dZ+\int_{-b}^{-d}g\varepsilon\frac{\partial \eta}{\partial x}dZ\\&+\int_{-b}^{-d}g(\varepsilon-1)\frac{\partial d}{\partial x}dZ\\&=\frac{\partial}{\partial t}\int_{-b}^{-d}udZ+\frac{\partial}{\partial x}\int_{-b}^{-d}u^2dZ+\frac{\partial}{\partial y}\int_{-b}^{-d}uvdZ+g\varepsilon\frac{\partial \eta}{\partial z}(b-d)\\&+g(\varepsilon-1)\frac{\partial d}{\partial x}(b-d)\end{aligned}\right\} \quad (56)$$

$$\left.\begin{aligned}&\int_{-b}^{-d}\frac{1}{\rho_l}\left(\frac{\partial \tau_{xx}}{\partial x}+\frac{\partial \tau_{xy}}{\partial y}+\frac{\partial \tau_{xz}}{\partial z}\right)dZ\\&=\frac{\partial \tau_{xx}}{\partial_x}(b-d)+\frac{\partial \tau_{xy}}{\partial y}(b-d)+\tau_{xzd}-\tau_{xzb}\end{aligned}\right\} \quad (57)$$

where, the shear stresses are expressed as follows:

$$\tau_{xy}=\mu\left(\frac{\partial v}{\partial x}+\frac{\partial u}{\partial y}\right) \quad (58)$$

$$\tau_{yy}=\mu\left(\frac{\partial v}{\partial y}+\frac{\partial v}{\partial y}\right)=2\mu\frac{\partial u}{\partial y} \quad (59)$$

$$\tau_{xx}=\mu\left(\frac{\partial u}{\partial x}+\frac{\partial u}{\partial x}\right)=2\mu\frac{\partial u}{\partial x} \quad (60)$$

Also, it is assumed that the shear stresses at the interface and the bottom are proportional to the velocity, the shear stresses can be given as follows:

$$\tau_{xzd} = \mu\left(\frac{\partial w}{\partial x} + \frac{\partial u}{\partial z}\right) \simeq C_b^{''}(U_1 - V_1) \tag{61}$$

$$\tau_{xzb} = \mu\left(\frac{\partial w}{\partial x} + \frac{\partial u}{\partial z}\right) \simeq C_b^{'''} V_2 \tag{62}$$

where, V_1 is the velocity component of the lower layer in the x direction and V_2 is the velocity component of the lower layer in the y direction.

By substituting Eqs. (58), (59), (60), (61) and (62) into Eq. (57), then Eq. (56) is expressed as follows:

$$\left.\begin{aligned} &\frac{\partial}{\partial t}\int_{-b}^{-d} u dZ + \frac{\partial}{\partial x}\int_{-b}^{-d} u^2 dZ + \frac{\partial}{\partial y}\int_{-b}^{-d} uv dZ + g\varepsilon\frac{\partial \eta}{\partial x}(b-d) \\ &+g(\varepsilon-1)\frac{\partial d}{\partial x}(b-d) - \frac{\mu}{\rho_l}(b-d)\left\{\frac{\partial}{\partial x}\left(2\frac{\partial u}{\partial x}\right) + \frac{\partial}{\partial y}\left(\frac{\partial v}{\partial x} + \frac{\partial u}{\partial y}\right)\right\} \\ &-\frac{1}{\rho_l}C_b^{''}(U_1 - V_1) + \frac{1}{\rho_l}C_b^{'''} V_2 = 0 \end{aligned}\right\} \tag{63}$$

The momentum correction coefficients of the lower layer are given as follows:

$$\beta_{xx} = \frac{1}{(b-d)U^2}\int_{-b}^{-d} u^2 dZ \tag{64}$$

$$\beta_{xy} = \frac{1}{(b-d)UV}\int_{-b}^{-d} uv dZ \tag{65}$$

Substituting Eqs. (26), (27), (64) and (65) into Eq. (63), assuming that μ is constant for the depth in the x, y directions and that β_{xx} and β_{xy} are 1, respectively, the result is defined as follows:

$$\left.\begin{aligned} &\frac{\partial U}{\partial t} + U\frac{\partial U}{\partial x} + V\frac{\partial U}{\partial y} + g\varepsilon\frac{\partial \zeta}{\partial x} + g(\varepsilon-1)\frac{\partial d}{\partial x} - \nu_e^l\frac{\partial}{\partial x}\left(2\frac{\partial U}{\partial x}\right) \\ &-\nu_e^l\frac{\partial}{\partial y}\left(\frac{\partial V}{\partial x} + \frac{\partial U}{\partial y}\right) - \frac{C''_b}{\rho_l(b-d)}(U_1 - V_1) + \frac{C_b^{'''}}{\rho_l(b-d)}V_2 = 0 \end{aligned}\right\} \tag{66}$$

where, $\nu_e^l \left(= \frac{\mu}{\rho_l}\right)$ is the eddy viscosity of the lower layer.

The stresses of the interface and the bottom are considered to be linear, these are expressed as follows:

$$\beta_m = \frac{C''_b}{\rho_l(b-d)} = \frac{f_m}{\rho_l(b-d)}\sqrt{(U_1-V_1)^2+(U_2-V_2)^2} \tag{67}$$

$$\gamma_m = \frac{C'''_b}{\rho_l(b-d)} = \frac{f_b}{\rho_l(b-d)}\sqrt{V_1^2+V_2^2} \tag{68}$$

where, f_b is the friction coefficient of the bottom.

From an analogous development, the y component of the momentum equation can be yielded, and by using Einstein notation, the momentum equation of the lower layer is therefore obtained as follows:

$$\left.\begin{aligned}\dot{V} + V_j V_{i,j} + \varepsilon g\eta_{,i} - (1-\varepsilon)gd_{,i} - \nu_e^l\left(V_{i,j}+V_{j,i}\right)_{,j} \\ +\beta_m(U_i - V_i) + \gamma_m V_i = 0\end{aligned}\right\} \tag{69}$$

Therefore, the continuity equations (Eq. (18) and Eq. (29)) and the momentum equations (Eq. (52) and Eq. (69)) will be considered in the following finite element models.

2.4 Finite Element Equations

2.4.1 Spatial Discretization

Let V be a flow domain. The continuity equations and the momentum equations are employed to the two layer current model in shallow water using Galerkin method for the discretization of the spatial unknown variables.

For the continuity equations (Eq. (18) and Eq. (29)) and the momentum equations (Eq. (52) and Eq. (69)) are employed, multiplying both sides of basic equations by the weighting functions and integrating over the domain V, the finite element solution equations can be derived as follows:

$$M_{\alpha\beta}\left(\dot{\eta}_\beta + \dot{d}_\beta\right) + B_{\alpha\beta i\gamma}\, U_{\beta i}\left(\eta_\gamma + d_\gamma\right) + C_{\alpha\beta\gamma i}\, U_{\beta i}\left(\eta_\gamma + d_\gamma\right) = 0 \tag{70}$$

$$M_{\alpha\beta}\,\dot{d}_\beta + B_{\alpha\beta i\gamma}\, V_{\beta i}\left(d_\gamma - b_\gamma\right) + C_{\alpha\beta\gamma i}\, V_{\beta i}\left(d_\gamma - b_\gamma\right) = 0 \tag{71}$$

$$\left.\begin{aligned} &M_{\alpha\beta}\,\dot{U}_{\beta i} + K_{\alpha\beta\gamma j}\, U_{\beta i} U_{\gamma i} + gH_{\alpha\beta i}\,\eta_\beta \\ &+\nu_e^u R_{\alpha j\beta j}\, U_{\beta i} + \nu_e^u S_{\alpha j\beta i}\, U_{\beta j} + M_{\alpha\beta}\,\alpha_m\left(U_{\beta i} - V_{\beta i}\right) = 0 \end{aligned}\right\} \tag{72}$$

$$\left.\begin{aligned} &M_{\alpha\beta}\,\dot{V}_{\beta i} + K_{\alpha\beta\gamma j}\, V_{\beta j} V_{\gamma i} + \varepsilon g H_{\alpha\beta i}\,\eta_\beta - (1-\varepsilon) g H_{\alpha\beta i}\, d_\beta + \nu_e^l R_{\alpha j\beta j}\, V_{\beta i} \\ &+\nu_e^l S_{\alpha j\beta i}\, V_{\beta j} - M_{\alpha\beta}\,\beta_m\left(U_{\beta i} - V_{\beta i}\right) + M_{\alpha\beta}\,\gamma_m V_{\beta i} = 0 \end{aligned}\right\} \tag{73}$$

where, coefficient matrices are expressed as follows:

$$\left.\begin{aligned} M_{\alpha\beta} &= \int_v \left(\Phi_\alpha \Phi_\beta\right) dV\,, \quad K_{\alpha\beta\gamma j} = \int_v \left(\Phi_\alpha \Phi_\beta \Phi_{\gamma,j}\, dV\right. \\ H_{\alpha\beta i} &= \int_v \left(\Phi_\alpha \Phi_{\beta,i}\right) dV\,, \quad R_{\alpha j\beta j} = \int_v \left(\Phi_{\alpha,j} \Phi_{\beta,j}\right) dV \\ S_{\alpha j\beta i} &= \int_v \left(\Phi_{\alpha,j} \Phi_{\beta,i}\right) dV\,, \quad B_{\alpha\beta i\gamma} = \int_v \left(\Phi_\alpha \Phi_{\beta,i} \Phi_\gamma\right) dV \\ C_{\alpha\beta\gamma i} &= \int_v \left(\Phi_\alpha \Phi_\beta \Phi_{\gamma,i}\right) dV \end{aligned}\right\}$$

In the above equations, Φ_α denotes linear triangular shape function.

2.4.2 Time Discretization

The differential terms with regard to time are included in Eqs. (70), (71), (72) and (73), and these equations are discretized using the Lax-Wendroff scheme (Kawahara, 1976).

The first step:

$$\left.\begin{aligned}\bar{M}_{\alpha\beta}\,U_\beta^{n+1/2} = \tilde{M}_{\alpha\beta}\,U_\beta^n - \frac{\Delta t}{2}[K_{\alpha\beta\gamma}\,U_\beta^n U_\gamma^n + gH_{\alpha\beta}\,Z_\beta^n \\ +\nu_e^u R_{\alpha\beta}\,U_\beta^n + \nu_e^u S_{\alpha\beta}\,U_\beta^n + \alpha_m M_{\alpha\beta}\left(U_\beta^n - V_\beta^n\right)]\end{aligned}\right\} \quad (74)$$

$$\left.\begin{aligned}\bar{M}_{\alpha\beta}\left(Z_\beta^{n+1/2} + D_\beta^{n+1/2}\right) = \tilde{M}_{\alpha\beta}\left(Z_\beta^n + D_\beta^n\right) \\ -\frac{\Delta t}{2}\left[B_{\alpha\beta\gamma}\,U_\beta^n\left(Z_\gamma^n + D_\gamma^n\right) + C_{\alpha\beta\gamma}\,U_\beta^n\left(Z_\gamma^n + D_\gamma^n\right)\right]\end{aligned}\right\} \quad (75)$$

$$\left.\begin{aligned}\bar{M}_{\alpha\beta}\,V_\beta^{n+1/2} = \tilde{M}_{\alpha\beta}\,V_\beta^n - \frac{\Delta t}{2}[K_{\alpha\beta\gamma}\,V_\beta^n V_\gamma^n \\ +H_{\alpha\beta}\{\varepsilon g Z_\beta^n - (1-\varepsilon) g D_\beta^n\} + \nu_e^l R_{\alpha\beta}\,V_\beta^n \\ +\nu_e^l S_{\alpha\beta}\,V_\beta^n - \beta_m M_{\alpha\beta}\left(V_\beta^n - V_\beta^n\right) + \gamma_m M_{\alpha\beta}\,V_\beta^n]\end{aligned}\right\} \quad (76)$$

$$\bar{M}_{\alpha\beta}\,D_\beta^{n+1/2} = \tilde{M}_{\alpha\beta}\,D_\beta^n - \frac{\Delta t}{2}\left[B_{\alpha\beta\gamma}\,V_\beta^n\left(D_\beta^n - B_\beta^n\right) + C_{\alpha\beta\gamma}\,V_\beta^n\left(D_\gamma^n - B_\beta^n\right)\right] \quad (77)$$

The second step:

$$\left.\begin{aligned}\bar{M}_{\alpha\beta}\,U_\beta^{n+1} = \tilde{M}_{\alpha\beta}\,U_\beta^n - \Delta t[K_{\alpha\beta\gamma}\,U_\beta^{n+1/2} U_\gamma^{n+1/2} + gH_{\alpha\beta}\,Z_\beta^{n+1/2} \\ +\nu_e^u R_{\alpha\beta}\,U_\beta^{n+1/2} + \nu_e^u S_{\alpha\beta}\,U_\beta^{n+1/2} + \alpha_m M_{\alpha\beta}\left(U_\beta^{n+1/2} - V_\beta^{n+1/2}\right)]\end{aligned}\right\} \quad (78)$$

$$\left.\begin{aligned}\bar{M}_{\alpha\beta}\left(Z_\beta^{n+1} + D_\beta^{n+1}\right) = \tilde{M}_{\alpha\beta}\left(Z_\beta^n + D_\beta^n\right) \\ -\Delta t\left[B_{\alpha\beta\gamma}\,U_\beta^{n+1/2}\left(Z_\gamma^{n+1/2} + D_\gamma^{n+1/2}\right) + C_{\alpha\beta\gamma}\,U_\beta^{n+1/2}\left(Z_\gamma^{n+1/2} + D_\gamma^{n+1/2}\right)\right]\end{aligned}\right\} \quad (79)$$

$$\left.\begin{aligned}\bar{M}_{\alpha\beta}\,V_\beta^{n+1} = \tilde{M}_{\alpha\beta}\,V_\beta^n - \Delta t[K_{\alpha\beta\gamma}\,V_\beta^{n+1/2} V_\gamma^{n+1/2} \\ +H_{\alpha\beta}\left\{\varepsilon g Z_\beta^{n+1/2} - (1-\varepsilon) g D_\beta^{n+1/2}\right\} + \nu_e^l R_{\alpha\beta}\,V_\beta^{n+1/2} \\ +\nu_e^l S_{\alpha\beta}\,V_\beta^{n+1/2} - \beta_m M_{\alpha\beta}\left(V_\beta^{n+1/2} - V_\beta^{n+1/2}\right) + \gamma_m M_{\alpha\beta}\,V_\beta^{n+1/2}]\end{aligned}\right\} \quad (80)$$

$$\left.\begin{aligned}\bar{M}_{\alpha\beta}\, D_{\beta}^{n+1} = \tilde{M}_{\alpha\beta}\, D_{\beta}^{n} - \Delta t[B_{\alpha\beta\gamma}\, V_{\beta}^{n+1/2}\left(D_{\beta}^{n+1/2} - B_{\beta}^{n+1/2}\right) \\ + C_{\alpha\beta\gamma}\, V_{\beta}^{n+1/2}\left(D_{\gamma}^{n+1/2} - B_{\beta}^{n+1/2}\right)]\end{aligned}\right\} \quad (81)$$

In the above equations $\bar{M}$ means lumped coefficient matrix. And $\tilde{M}$ is the mixed coefficient which is calculated as:

$$\tilde{M} = e\bar{M} + (1 - e)M \quad (82)$$

where, e is lumping parameter.

From the equations as described above, the unknown variables can be solved simultaneously.

CHAPTER 3
MOVING BOUNDARY

From the finite element equations, the interface level d between the upper and lower layer can be calculated on each nodal point. If the interface level is higher than the depth of the sea bed on the domain at all time, the moving boundary of the lower layer is not necessary, but the case that the interface level is set to be under the minimum depth of the sea bed, the analytical area of the lower layer is changeable by the interface level getting higher or lower. In this chapter, for the changeable area of the lower layer, the moving boundary method is applied to this model, so that the analytical area is defined two kind of area as the single layer area and the two layer area.

3.1 Judgment of Elements

The analytical area of the lower layer is decided by the presence of interface level on each nodal point. If the calculated interface level d is higher than the depth of the sea bed at one nodal point, it is assumed that the water level of lower layer exists at that point (wet nodal point). Otherwise, it is assumed that the water level of lower layer doesn't exist (dry nodal point). Then, if every three nodal points of one element are wet nodal point, the element is included in the two layer area. If one nodal point at least is dry element, the element is included in the single area. Also, the waterside element is defined as that the element which has both wet and dry nodal point. For example, as shown in Fig. 3, elements from 1 to 24 are included in the two layer area, and elements from 25 to 36 are included in the single layer area.

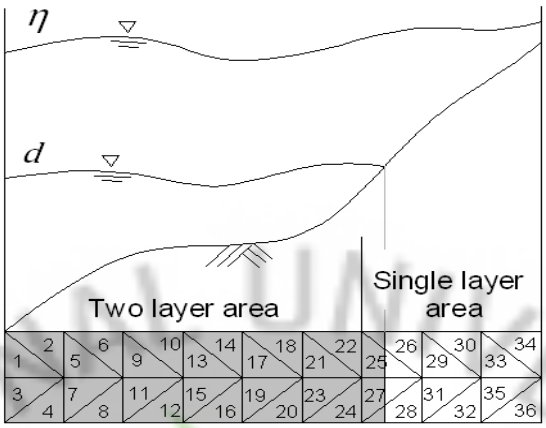

Fig. 3 Judgment of element

3.2 Treatment of the Analytical Area

The elements of the two layer area, which has the lower layer, are calculated by two layer current model, and the others including waterside elements are calculated by shallow water model. Then, the calculated interface level is compared with the depth of the sea bed each time, and the analytical area is redefined as the single area and the two layer area. The boundary of the lower layer is defined newly when the lower area is changed, and the normal velocity of the lower layer is set to be 0.

3.3 Algorithm of Wetting and Drying

The algorithm of the analysis considering moving boundary is shown as follows:

1. Check the interface level d^n on the nodal points of the two layer area.

2. In the waterside element, if the averaged interface level of three nodal points is higher than the depth of the sea bed on the dry nodal point, which is defined wet nodal point. (The interface level of the dry nodal point is set to be its depth of the sea bed when the averaged interface level is calculated)
3. If three nodal points of one element are wet nodal point ($d < b$), include the element in the two layer area.

   If any nodal point of one element is dry nodal point ($d_i \geq b_i$), include the element in the single layer area.
4. Do the step 2 for all elements.
5. Compute $U^{n+1}, V^{n+1}, \eta^{n+1}, d^{n+1}$ by finite element equations..
6. Define the boundary nodal points of the lower layer, and apply the boundary condition.
7. Set $n = n + 1$, and go to 1.

CHAPTER 4
VERIFICATIONS OF THE NUMERICAL MODEL

In this chapter, to verify two layer current model, the numerical model by two layer current of Jumunjin fishery port where SEB has been established is carried out, and the computed results are compared with the observed data.

4.1 Application of Jumunjin Fishery Port

For the application of two layer current model, the numerical model of Jumunjin fishery port is carried out. For the study area, a 3D bottom bathymetry is shown in Fig. 4. Due to the shallow water depth in the flow domain, the interface level is assumed 3m under the mean sea level at the initial time. Thus, the upper layer and lower layer are defined by the interface level, respectively.

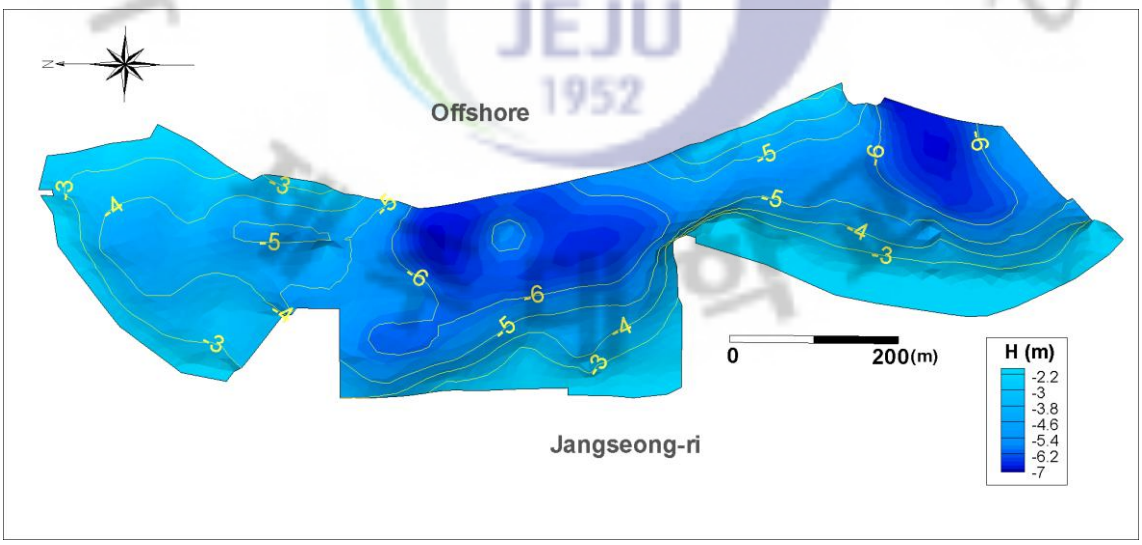

Fig. 4 3D bottom bathymetry in Jumunjin fishery port

With the boundary conditions, it is assumed that the normal velocity to the coastline is zero, and the elevations of incident waves are assumed on the entrance of the port to be given by

$$\eta = \sum_{m=1}^{Nc} \left[\alpha_m^u \, sin\left\{ \frac{2\pi}{T_m} \, t - \kappa_{\mathrm{m}} \right\} + \alpha_m^l \, sin\left\{ \frac{2\pi}{T_m} \, t - \kappa_{\mathrm{m}} \right\} \right] \; on \; \Gamma_o^u \tag{83}$$

$$d = d_t - \sum_{m=1}^{Nc} \left[\alpha_m^l \, sin\left\{ \frac{2\pi}{T_m} \, t - \kappa_{\mathrm{m}} \right\} \right] \quad on \; \Gamma_o^l \tag{84}$$

where N_c is the incident waves number, a_m is the amplitude, κ_m is the phase delay, T_m is the period of M_2, S_2, K_1 and Q_1 constituent, t is the time increment in computation and d_t is the depth from the mean sea level to the interface level at t, respectively. The harmonic analysis of M_2, S_2, K_1 and Q_1 in Jumunjin fishery port is shown in Table 1.

Table 1. The results of the harmonic analysis for tide in Jumunjin fishery port (MOMAF, 1999)

N_c	Constituent	Amplitude $\alpha_m \; (cm)$	Period $T_m \; (hour)$	Phase delay $\kappa_m \; (degree)$
1	M_2	6.94	12.4206	91.486
2	S_2	1.79	12.0000	120.689
3	K_1	4.35	23.9344	1.367
4	O_1	4.70	25.8193	320.935

The computational mesh of the upper layer and lower layer are consisted of 5230 triangular elements with 2784 nodal points, and 3029 triangular elements with 1653 nodal points, respectively, as shown in Fig. 5.

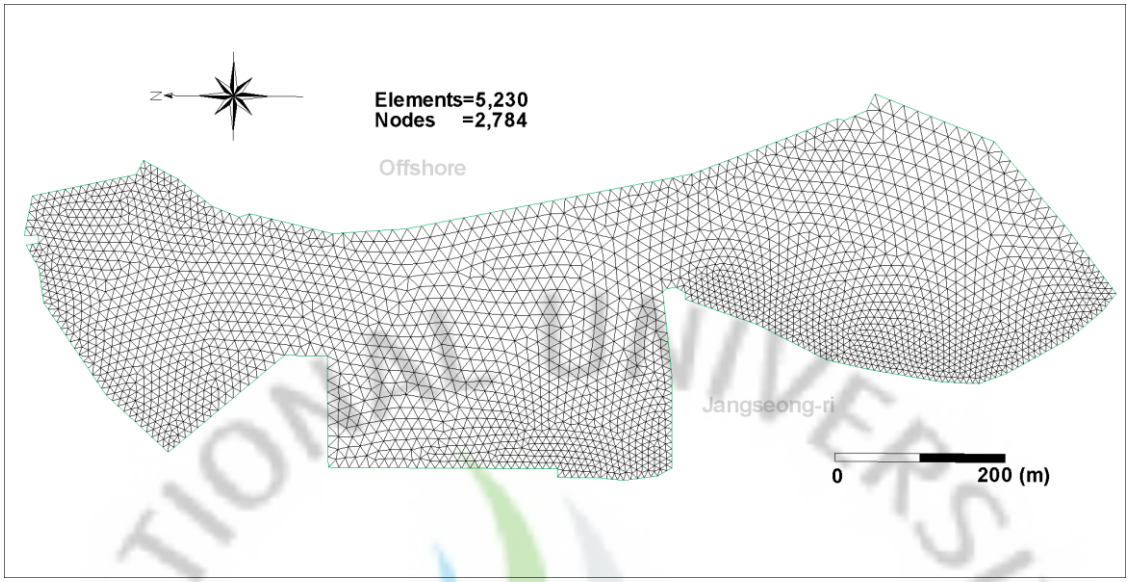

< Upper layer >

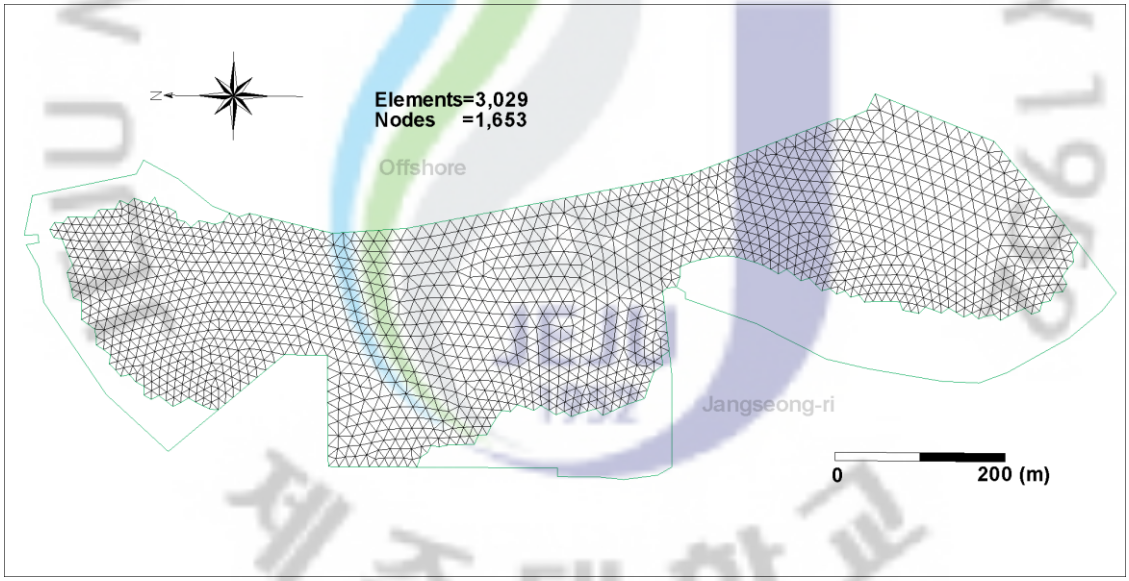

< Lower layer >

Fig. 5 Finite element idealization of Jumunjin fishery port

Fig. 6 and Fig. 7 show the velocity of flow vectors at the flood tide and the ebb tide. It shows that the tidal flow pattern is simulated well in both layers, and that the moving boundary can be applied in this model. Due to the weak tidal current in East Sea where Jumunjin fishery port is located, the velocities of the flow field are smaller than $1\,cm/s$ overall, these results are in good agreement with the computed results by MOMAF(1999). The velocity near the entrance of the port is little strong, relatively, but the others are weak. Therefore, the deteriorated water quality of Jumunjin fishery port may be caused by the weak tidal current.

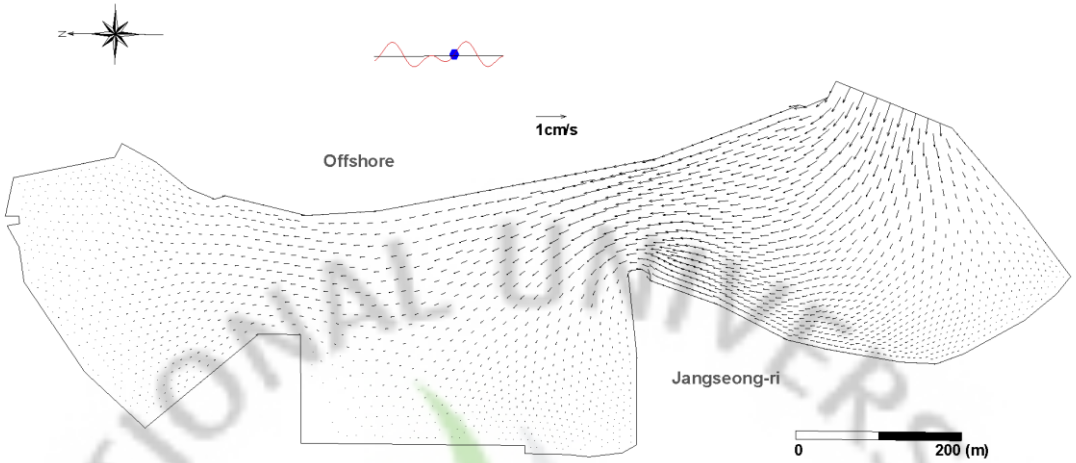

< Upper layer >

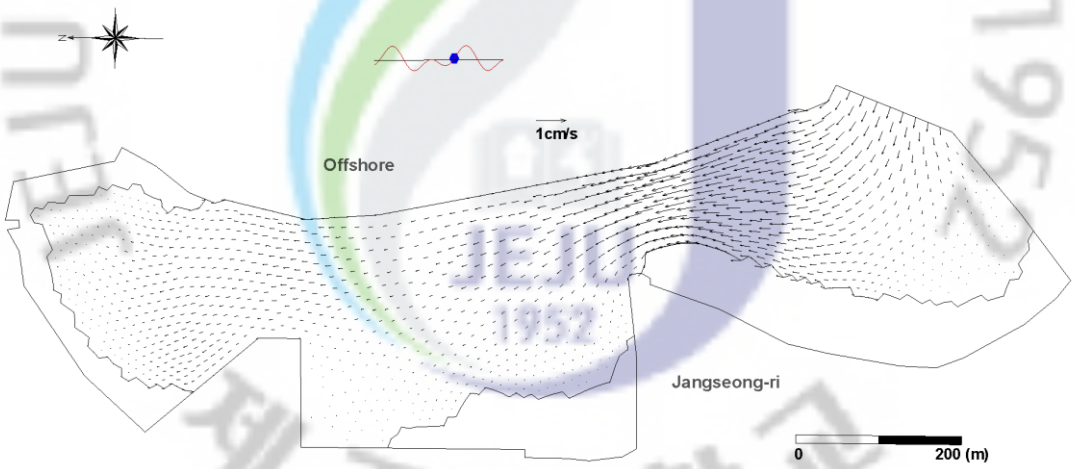

< Lower layer >

Fig. 6 Velocity vectors of Jumunjin fishery port at flood tide

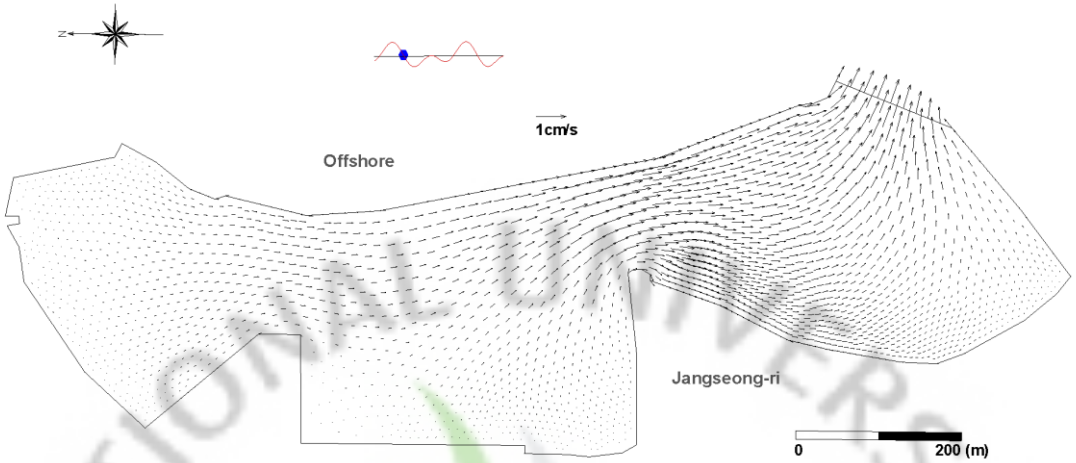

< Upper layer >

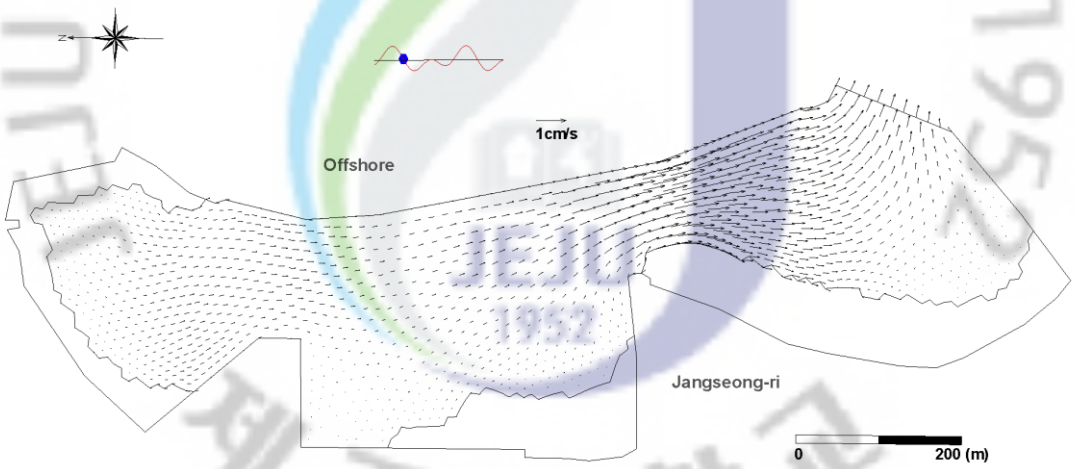

< Lower layer >

Fig. 7 Velocity vectors of Jumunjin fishery port at ebb tide

4.2 Verification of Jumunjin Fishery Port with SEB

As the next verification model, when the seawater from the outside area flows in the port by the SEB, the numerical model by two layer current is carried out. The calculation conditions and the boundary conditions are the same as the above verification model. Inflow condition of seawater from SEB is given by $77.38cm^3/s$ flux, which was observed by Sea Tech R&D (2008). In this study, as the SEB uses the waves overflowed a wall of arch, it is assumed that the water of the upper layer is exchanged the seawater while the sea level is higher than mean sea level, and the flux of the inflow is set to be maximum value at the high tide.

Fig. 8 shows the velocity of flow vectors by the SEB at the high tide. For the weak tidal current, the inflow from the SEB is flowed toward the entrance of the port. Except portion of inside area, this figure shows good water exchanging of Jumunjin fishery port.

To verify two layer current model of this case, the computed results are compared with the observed data by Sea Tech R&D (2008) at the nodal points in Fig. 9. For the depth of the seabed at the nodal points of SC-1 and SC-2 is shallower than the interface level, these velocities of the lower layer cannot be calculated in this case. The comparisons of these velocities are shown in Table 2, it shows that the results of two layer current are in good agreement with the observed data.

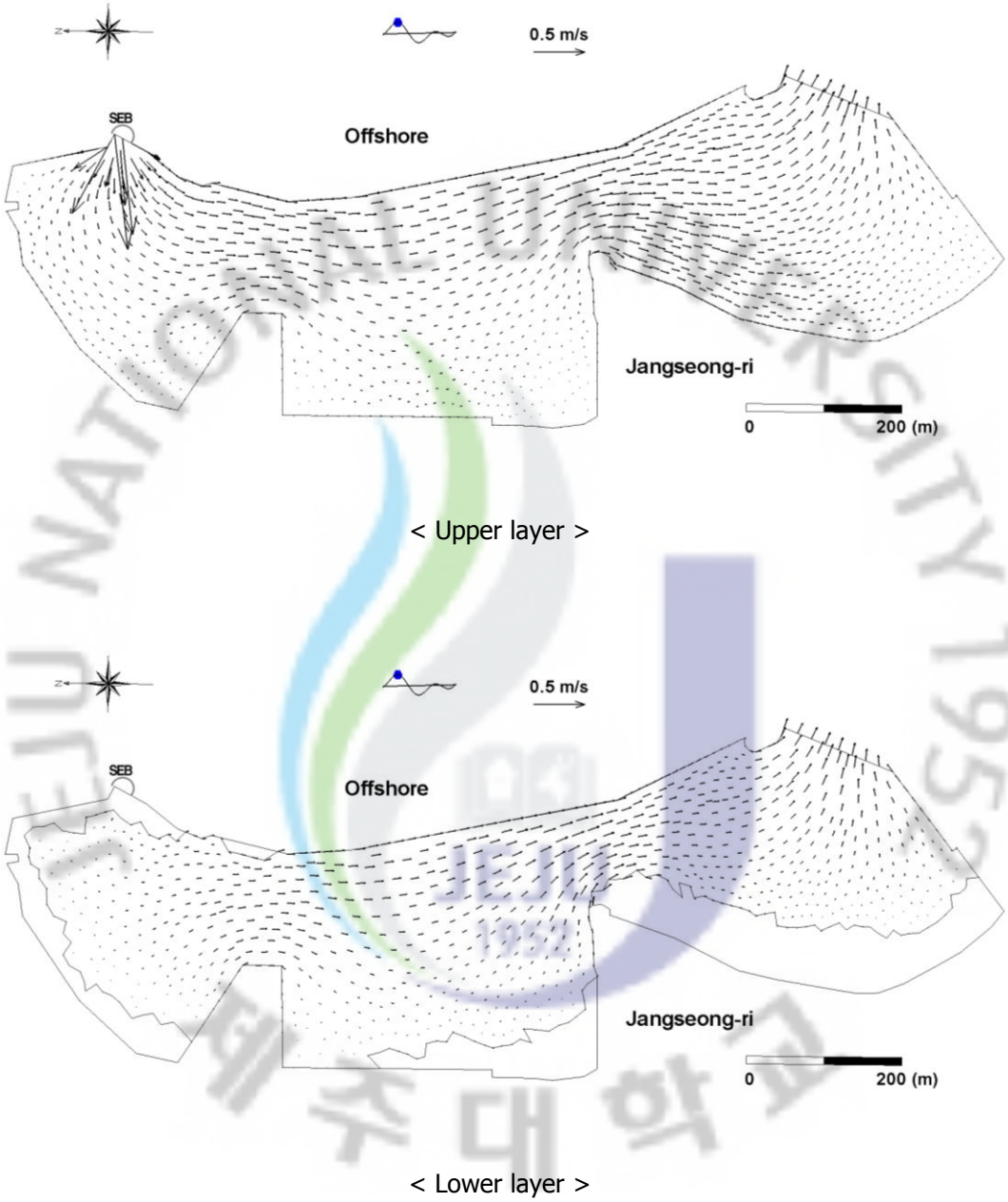

Fig. 8 Velocity vectors of Jumunjin fishery port with SEB

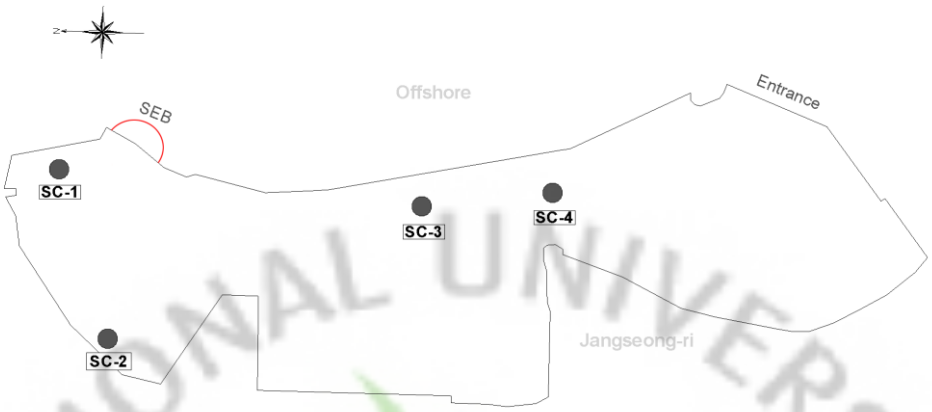

Fig. 9 Observed nodal points

Table 2. Comparison of velocity with computed results and observed data

Node	Observed Data (Averaged) (cm/s)		Present Method (cm/s)	
	Upper	Lower	Upper	Lower
SC-1	3.32	3.20	3.36	-
SC-2	1.76	1.70	1.49	-
SC-3	10.87	9.90	9.49	8.10
SC-4	12.46	10.39	12.94	10.83

CHAPTER 5
APPLICATIONS OF THE NUMERICAL MODEL WITH MANIFOLD CHANNEL

In this chapter, for the practical use of Manifold channel, a virtual manifold channels are assumed in Jumunjin fishery port, and the numerical model by two layer current is carried out. Also, to examine the effect of gate condition in Manifold channel, five cases of manifold channels are assumed and the numerical model is simulated.

5.1 Application of Jumunjin Fishery Port with Manifold Channel

5.1.1 Numerical Analysis Conditions

Fig.10 shows the finite mesh idealization of Jumunjin fishery port with manifold channels. The computational mesh of the upper layer and lower layer are consisted of 2901 triangular elements with 1740 nodal points, and 1661 triangular elements with 950 nodal points, respectively. As shown in this figure, in this case, it is assumed that three of the gates are located inside of the port where the seawater is not exchanged by the SEB well. The manifold channels are assumed length of 762.1m, width of 5.3m and depth of 2.0m., and in order of the counter clockwise, the gates are named as Gate 1, Gate 2 and Gate 3. The calculation conditions and the inflow condition are also the same as the SEB case.

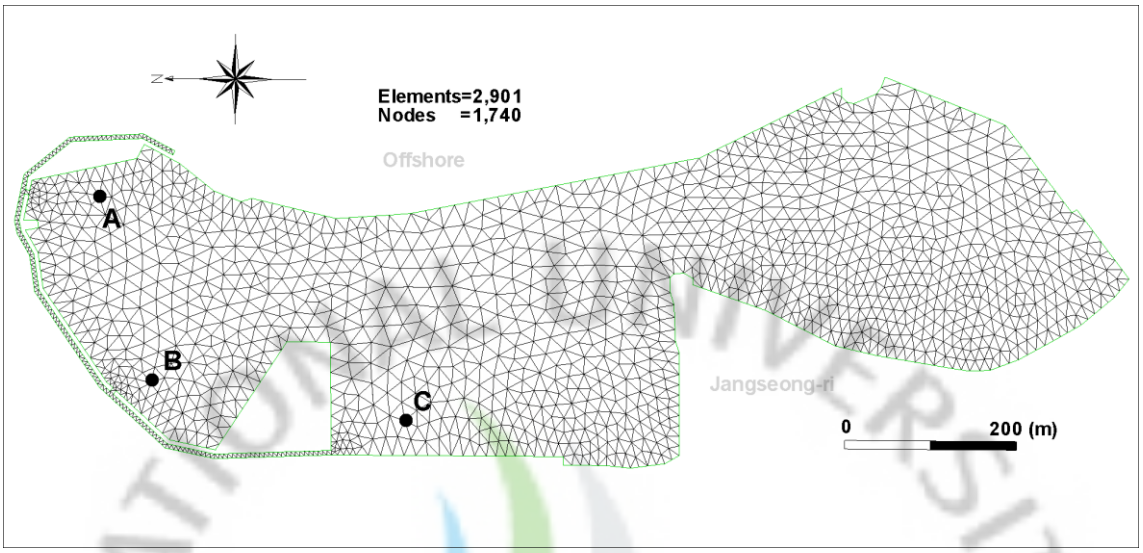

< Upper layer >

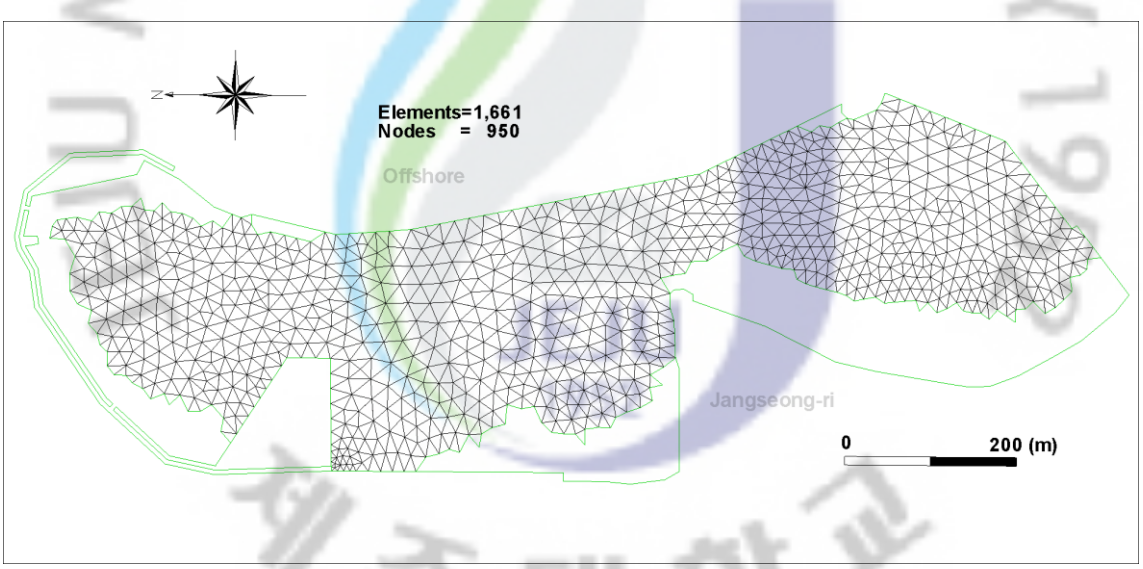

< Lower layer >

Fig. 10 Finite element idealization of Jumunjin fishery port with Manifold channel

5.1.2 Results of Numerical Model

Fig. 11 shows the velocity vectors of Jumunjin fishery port with manifold channels. It shows that the vortex of counter clockwise is weakly formed on the inside area. Due to the vortex and the various losses by the manifold channels, the velocity of the flow field is a little weaker than the SEB.

To examine the velocity of flow on the inside area definitely, at the nodal points as shown in Fig. 10, the comparisons of velocity with Manifold channel and the SEB are shown in Fig. 12. As the vortex of counter clockwise is occurred near the point A and the velocity on that area is not affected by the current of inflow from the SEB directly, it shows that the velocity at the nodal point A is weaker than the SEB. But the velocities at the nodal points B and C are stronger than SEB, it shows that Manifold channel has an advantage over the SEB for the water exchange of the inside area generally. Also, the vector diagrams at the nodal points are shown in Fig. 13, respectively. Though the velocity of the flow field is little weaker than the SEB, the flow pattern of the inside area is shifted by the inflow of the manifold channels, it shows that Manifold channel can be exchanged the water from the seawater of outside area throughout the inside area.

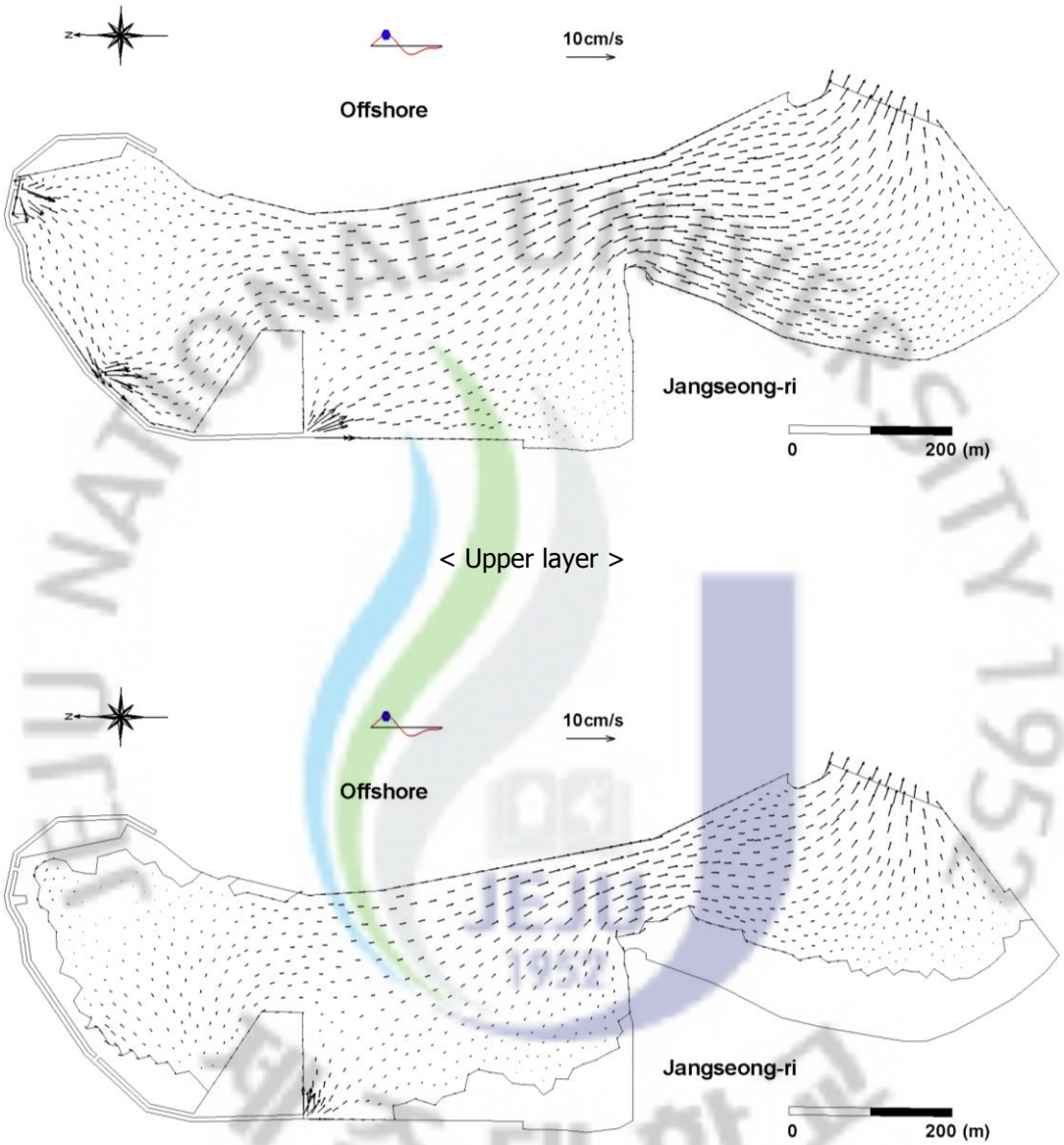

Fig. 11 Velocity vectors of Jumunjin fishery port with Manifold channel

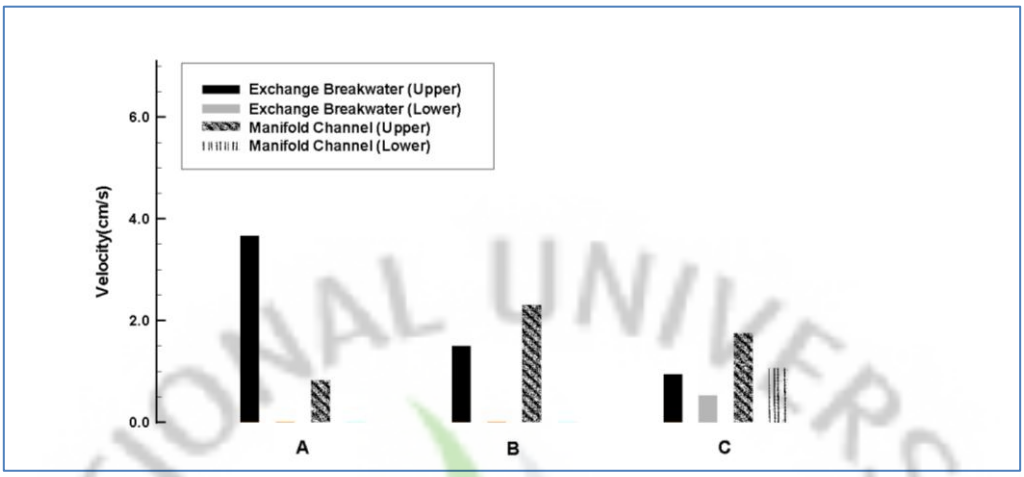

Fig. 12 Comparisons of velocity with Manifold channel and SEB at the nodal points A, B and C

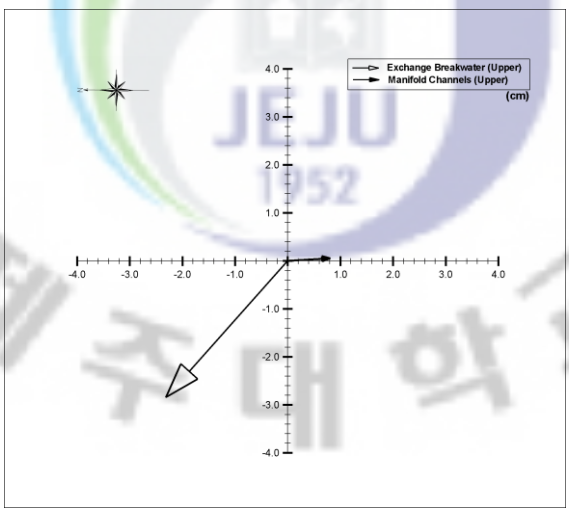

(a) nodal point at A

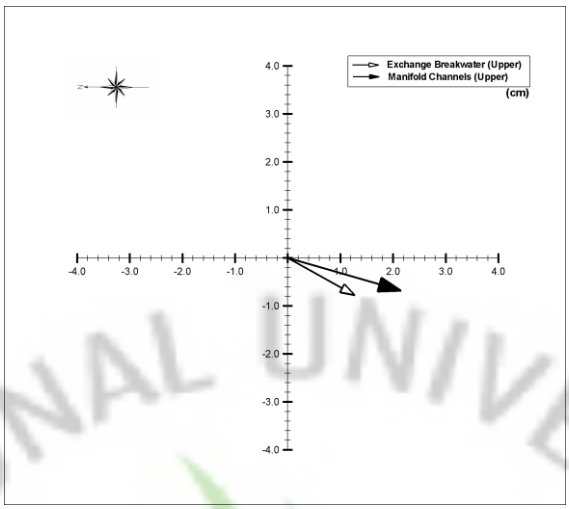

(b) nodal point at B

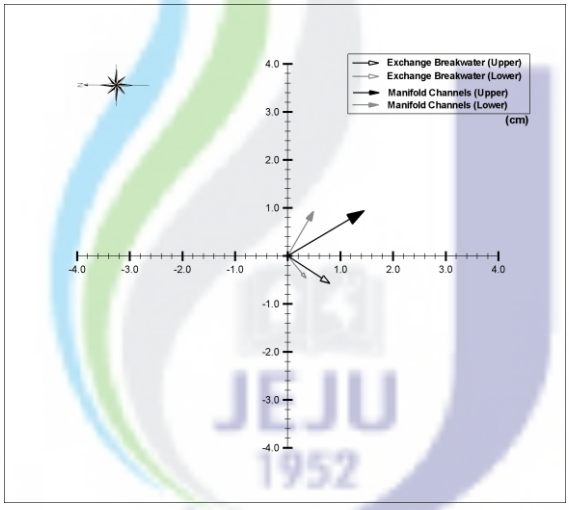

(c) nodal point at C

Fig. 13 Vector diagrams at nodal point A, B and C

5.2 Examination for Effects of Manifold Channel

5.2.1 Numerical Analysis Conditions by Outflow Gates

It is assumed that the five gates are located inside of the port as shown in Fig. 13, and the manifold channel is assumed length of 762.1m, width of 5.3m and depth of 2.0m. The calculation conditions by outflow gates of the manifold channels are given in Table 3.

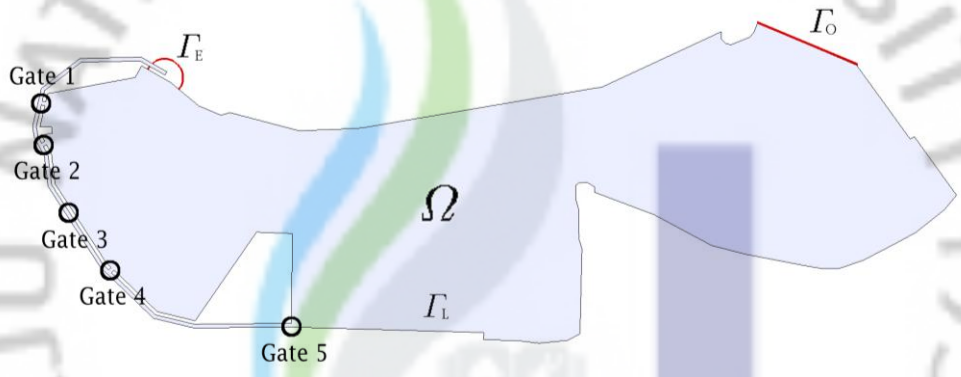

Fig. 14 Gate position of Manifold channel

Table 3. Calculation conditions by outflow gates of Manifold channel

Case	Gate1	Gate2	Gate3	Gate4	Gate5
Case 1	-	-	On	-	On
Case 2	-	On	On	On	On
Case 3	-	On	-	On	On
Case 4	On	On	-	On	On
Case 5	On	-	-	On	On

5.2.2 Results of Numerical Model

Fig. 14 shows the velocity vectors of Case 1. One of gates is located middle of inside area in order that the seawater is flowed toward the entrance of the port, but the vortex of counter clockwise is strongly formed, so that this case is not good for the water exchange.

Fig. 15 shows the velocity vectors of Case 2. The Gate 2 and Gate 4 are added on the Case 1 to control the vortex, but the vortex is still formed at the inside area.

Fig. 16 shows the velocity vectors of Case 3. Except the Gate 3, it shows that the vortex is weaker than before, but the velocity of inside area near the Gate 1 is also weak.

Fig. 17 shows the velocity vectors of Case 4. Gate 1 is added on the Case 3 to increase the velocity of inside area near the Gate 1. As the velocity of that area increases, the vortex is eliminated, but the velocity of inside area near the Gate 4 is weaker than before.

Fig. 18 shows the velocity vectors of Case 5. By using the Gate 1, Gate 4 and Gate 5, most of the velocity at the inside area can be increased, and the inflow of the seawater by the manifold channels flows toward the entrance of the port. Therefore, Case 5 is good for the water exchange of manifold channel among these cases.

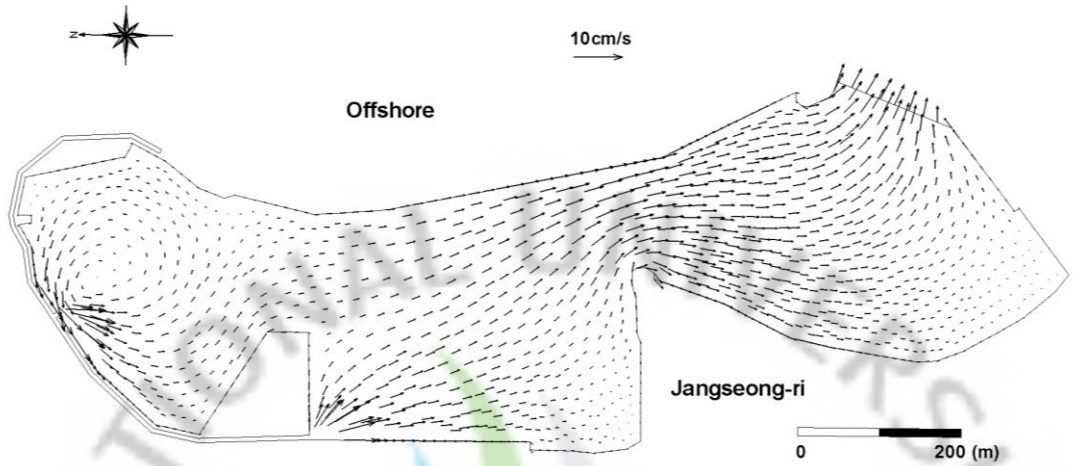

Fig. 15 Velocity vectors of upper layer in Case-1

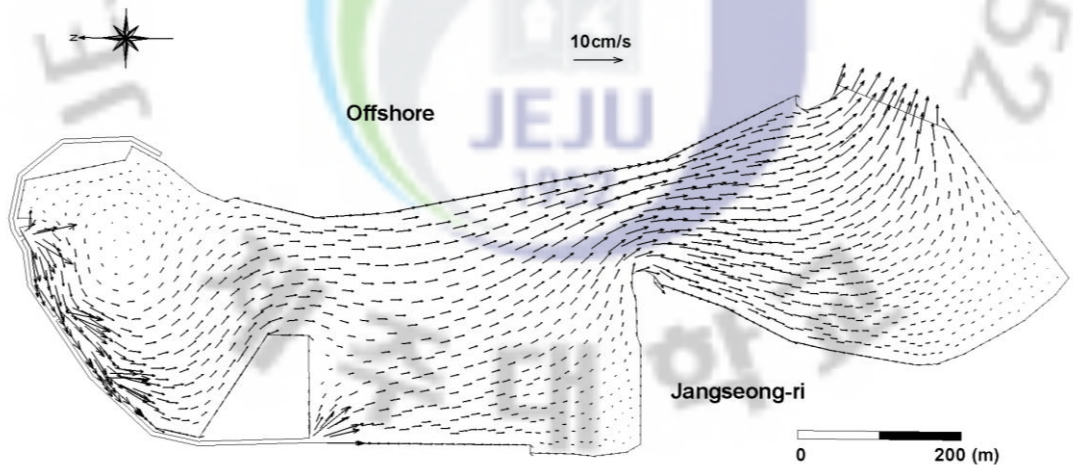

Fig. 16 Velocity vectors of upper layer in Case-2

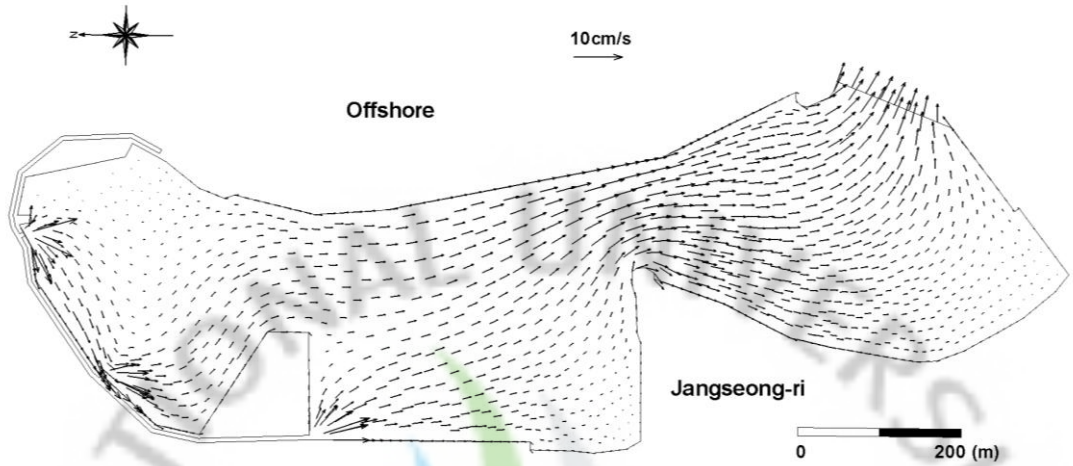

Fig. 17 Velocity vectors of upper layer in Case-3

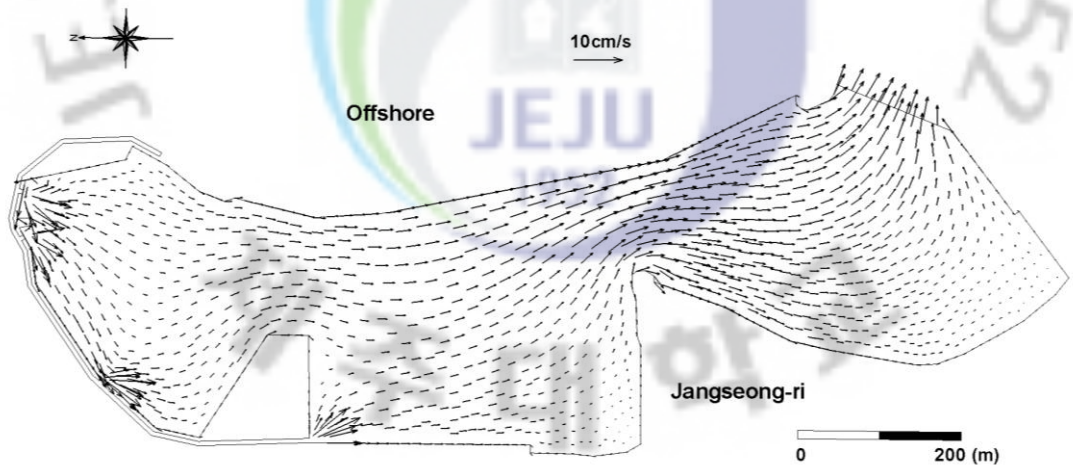

Fig. 18 Velocity vectors of upper layer in Case-4

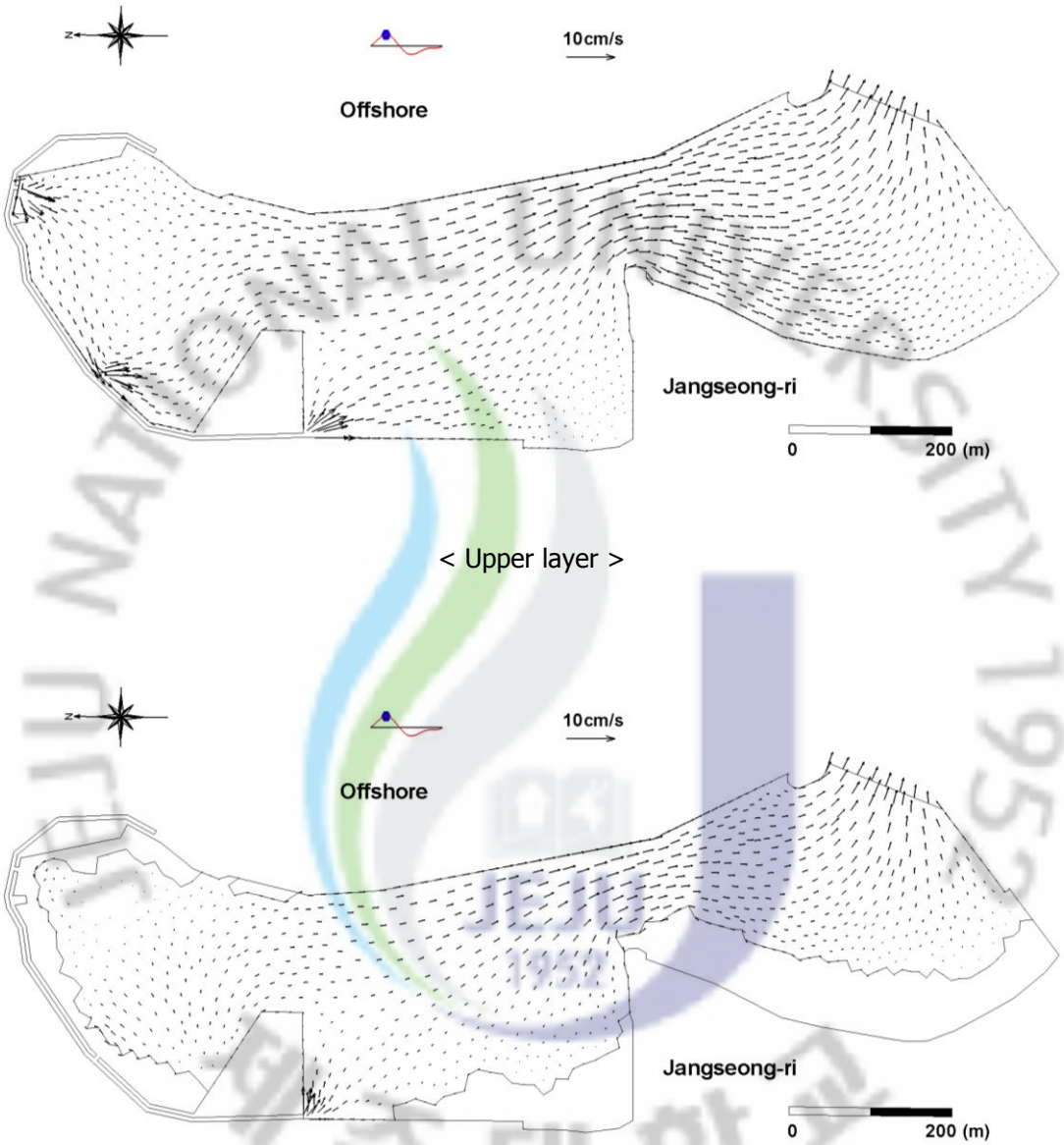

Fig. 19 Velocity vectors of upper and lower layer in Case-5

CHAPTER 6
CONCLUSIONS
AND FUTURE RESEARCH DIRECTIONS

6.1 Conclusions

In this study, Manifold channel, the new concept of the seawater exchange breakwater, is presented, and the numerical model by two layer current is applied. The main results of present study are listed below:

(1) By using the moving boundary method, the numerical model by two layer current for tidal current is carried out. It shows that the moving boundary of the lower layer can be applied in this model. The velocity of the port by the tidal current is weak, so that the water quality of inside area cannot be improved by the tidal current.

(2) To verify two layer current model, the computed result of the SEB is compared with observed data. It shows a good agreement between the results and the observed data. Thus, the numerical analysis by two layer current is verified.

(3) From the results of the chapter 5, it shows that the water of the inside area can be exchanged the seawater from outside area by the present method, and Manifold channel is to be a useful method for improving the water quality. However the velocity of the port is a little weaker than the SEB, there is a more need to investigate the manifold channels for the practical use.

(4) The effect of the gate conditions in Manifold channel is investigated by using this numerical model. From these results, the efficiency for the water exchange is greatly affected by the gate conditions.

(5) Due to the aspect of Jumunjin fishery port, the velocity of the inside area is correlated with the occurred vortex of the inside area. Thus, the relation caused by aspect of the port is obtained: as the vortex is formed, the velocity of the inside area near the Gate 4 is increased, while the velocity of the area near the Gate 1 is decreased.

As these results in this study, Manifold channel might be used broadly for the design of a breakwater to develop the facilities of port with waterfront area and water amenity.

6.2 Future Research Directions

For practical use of this method, there is a more need to investigate the manifold channels, and then the remaining works are listed as follows:

(1) For the application of the manifold channels, the losses of the manifold channels should be calculated, and the effective aspect conditions of the channel, such as length, width, depth and curve, should be defined. Then, the velocity by the inflow current should be increased.

(2) Much more in calculating cases about the gate positions are remained to be done. From these results, the standard equations about the gate position should be derived.

(3) To improve the propriety of the numerical analysis and to examine the water exchanging of the whole layers on port, multi-layer current model should be developed.

(4) The submerged gate should be considered, and also the effect of width and direction of the gate should be investigated.

References

Han, D.J. and Lee, D.S (2006). "Effect of water quality improvement by seawater exchange breakwater install." *Korean J. Sanitation*, Vol. 21, No. 3. pp.61~72 (in Korean).

Jung, T.S and Kim, C.S. (1992). "A finite element hydrodynamic model for moving boundary problems." *J. of Korean Soc. of Coastal and Ocean Eng.*, Vol. 4, No.3, pp. 146-155 (in Korean).

Kawahara, M. (1976). "Convergence of finite element Lax-Wendroff method for linear hyperbolic differential equation." *Proc. of JSCE*, No. 253, pp. 95-107.

Kasahara, K., Hara, H. and Kawahara, M. (1984). "Two-step explicit finite element method for two-layer flow analysis." *Int. J. Numer. Meth. Fluids*, Vol.4, pp. 931-947.

Kawahara, M., Hirano, H., Tsubota, K., and Inagaki, K. (1982). "Selective lumping finite element method for shallow water flow." *Int. J. Num. Meth. Fluids*, Vol. 2, pp. 89-112.

Kim, N.H. (1995). "An analysis of shallow water flow by two step explicit finite element scheme." *J. of the Korean Society of Civil Eng.*, Vol.15, No.6, pp. 1669-1677.

Kim, N.H. and Park, J.H. (2003). "The flow analysis of Jeju harbor using moving boundary technique." *J. of Korean Navigation and Port Research*, Vol. 27, No. 5, pp. 539-546 (in Korean).

Kim, N.H., Park, J.H., and Kang, H.W. (2007). "The numerical analysis of Jeju harbor flow considering effect of seasonal wind." *J. of Korean Navigation and Port Research*, Vol. 31, No. 9, pp. 793-799.

Kim, N.H., Yang, J.P. and Park S.G. (2000). "Automatic mesh generation method in shallow water area considering water depth." *J. of Korean Institute of Port Research*, Vol. 14, No. 1, pp. 97-105.

Kim, N.H., Yoon, H.C. and Hur, Y.T. (2006). "A technique development to generate triangular mesh using distinct element method." *Proc. of the Korean Annual Conference on Civil Engineering*, pp. 1498-1501 (in Korean).

Lee, D.S., Lee, C.H., Oh, Y.M., Chun, I.S. and Kim, C.I. (2003). "Comparison of the net inflow rates of seawater exchange breakwater of different shapes." Ocean and Polar Research, Vol. 25, pp. 393-397.

MOMAF (1999). *Research for exchange breakwater to practical use (I)* (in Korean).

MOMAF (1999). *Research for exchange breakwater to practical use (II)* (in Korean).

MOMAF (2000). *Research for exchange breakwater to practical use (III)* (in Korean).

Sea Tech R&D (2008). *Report of ocean survey for exchange breakwater on Jumunjin fishery port* (in Korean).

Shimada K. (1993). "Physically-based mesh generation: automated triangulation of surfaces and volumes via bubble packing." Ph.D. Dissertation, Massachusetts Institute of Technology, U.S.A.

Shimada, K. and Gossard, D.C. (1998). "Automatic triangular mesh generation of trimmed parametric surfaces for finite element analysis." Computer Aided Geometric Design, Vol. 15, No. 3, pp. 199-222.

Sloan, S.W. (1986). "A fast algorithm for constructing Delaunay triangulations in the plane." Adv. Eng. Software, 9(1), pp. 34-55.

Yoon, S.J. (2003). "Study on sea-water exchange and controlling sediment entertainment using breakwater with channel in a harbor." Ph.D. dissertation, University of Osaka, Japan (In Japaness).